scientific reports

Check for updates

OPEN

Ticam2 ablation facilitates monocyte exhaustion recovery after sepsis

Blake A. Caldwell[1], Susanti Ie[2], Amy Lucas[2] & Liwu Li[1,3]✉

Sepsis is a leading cause of death worldwide, with most patient mortality stemming from lingering immunosuppression in sepsis survivors. This is due in part to immune dysfunction resulting from monocyte exhaustion, a phenotype of reduced antigen presentation, altered CD14/CD16 inflammatory subtypes, and disrupted cytokine production. Whereas previous research demonstrated improved sepsis survival in *Ticam2*$^{-/-}$ mice, the contribution of TICAM2 to long-term exhaustion memory remained unknown. Using a cecal slurry injection sepsis model, we monitored the establishment and recovery of monocyte exhaustion in *Ticam2*$^{-/-}$ mice. After one week of recovery, we profiled bone marrow and splenic reservoir monocytes in *Ticam2*$^{-/-}$ mice and found that, in contrast to the persistent exhaustion observed in wild-type monocytes, *Ticam2*$^{-/-}$ monocytes largely resembled healthy controls. To determine the impact of TICAM2 ablation on innate epigenetic memory in sepsis, we measured genome-wide DNA methylation in bone marrow monocytes and found that *Ticam2*$^{-/-}$ cells exhibit a unique profile of altered methylation at CEBPE binding sites and regulatory features for key immune genes such as *Dmkn* and *Btg1*. Bearing human translational relevance, a case study of time course blood samples collected from a sepsis patient presenting with SIRS and a positive qSOFA revealed a similar effect in human monocytes, which steadily transition into an exhausted memory characterized by a CD38^{high}; CX3CR1^{low}; HLA-DR^{low} state within four days of hospital admittance. Together, our data reveal the chronic preservation of monocyte exhaustion, partially controlled by TICAM2.

Keywords Ticam2, Sepsis, Monocyte exhaustion, Innate immune memory

Sepsis accounts for 20% of all global deaths and remains the most expensive medical disorder to treat, with a combined annual cost of $38 billion in the United States alone.[1,2] This clinical burden is largely the result of long-term immunosuppression in sepsis survivors, with late-phase mortality from secondary infections accounting for roughly 75% of sepsis-associated deaths.[3,4] For this reason, therapies geared toward immune stimulation and memory resolution have become a major translational target in the treatment of long-term immune dysfunction in sepsis survivors.[5,6]

In the innate immune system, monocytes play essential roles in sepsis pathogenesis.[7,8] During the early phase of sepsis progression, monocytes contribute to systemic hyper-inflammation through the secretion of pro-inflammatory cytokines such as Tumor necrosis factor (TNF), Interleukin-1 beta (IL-1β), and Interleukin 6 (IL-6).[9] Shortly after the initial phase of inflammation, during the period of sustained immunoparalysis, monocytes exhibit signs of immune tolerance typified by reduced antigen presentation, altered CD14/CD16 inflammatory subtypes, impaired cytokine production, and broad transcriptional alterations.[10–14] During the chronic phase of sepsis recovery, monocytes adopt an exhausted state characterized by persistent pathogenic inflammation and immune suppression. This phenotype serves as an important biomarker in sepsis survivors, with exhausted monocyte expansion generally indicating a heightened susceptibility to secondary or nosocomial infection and worsened prognosis.[15–17].

Previous work from our laboratory demonstrated that signaling through Toll-like receptor 4 (TLR4) adaptor TICAM2 is a major upstream regulator of monocyte exhaustion.[12] Loss of TICAM2 in mice is associated with diminished T cell suppression by monocytes and increased survival during the initial hyper-inflammatory phase of sepsis.[18] *Ticam2* deletion also impacts the acquisition of epigenetic memory in monocytes cultured under repetitive endotoxin stimulation, diminishing histone H3 lysine 27 acetylation (H3K27ac) and 5-methylcytosine (5mC) reprogramming at gene enhancers.[19,20] However, despite these promising results, the effect of TICAM2 ablation on long-term monocyte exhaustion recovery in sepsis survivors remains to be determined.

[1]Department of Biological Sciences, Virginia Tech, Blacksburg, VA 24061-0910, USA. [2]Carillion Roanoke Memorial Hospital, Roanoke, VA 24014, USA. [3]Lead contact : Liwu Li. ✉email: lwli@vt.edu

To address this issue, we performed cecal slurry (CS) injections on *Ticam2*$^{-/-}$ mice and monitored monocyte recovery at the level of cell surface exhaustion markers, cytokine expression, and epigenetic memory. Our results demonstrate that TICAM2 deletion restores monocyte responses during the early phase of sepsis progression and accelerates the rate of exhaustion recovery relative to wild-type (WT) control mice. These results highlight the therapeutic potential TICAM2 suppression as a means of combatting long-term immunosuppression in sepsis survivors.

Results

Ticam2 deletion supports bone marrow niche and monocyte activity after sepsis

Ticam2 deletion was previously shown to increase the survival rate for sepsis-challenged mice.[18] To test how loss of TICAM2 impacts bone marrow niche monocytes during the acute phase response of sepsis, we performed sequential intraperitoneal CS injections on WT control C57BL/6 or *Ticam2*$^{-/-}$ mice and analyzed bone marrow cells by flow cytometry 48 h after sepsis onset (Fig. 1a). In addition to increasing the proportion of monocytes and neutrophils among bone marrow cells, CS injection led to an expansion of Ly6C-intermediate monocytes with a concomitant decrease in Ly6C-low and Ly6C-high subtypes in both WT and *Ticam2*$^{-/-}$ mice (**Supplemental** Fig. 1a-c).

Exhausted monocytes are characterized by reduced cell surface levels of antigen-presenting MHCII and chemokine receptor CX3CR1 and increased levels of the NAD metabolizing signaling molecule CD38.[11–13,21] This effect was observable in both WT and *Ticam2*$^{-/-}$ CS-injected mice, which also demonstrated elevated levels of scavenger receptor MARCO, an additional feature of exhausted cells (Fig. 1b**, Supplemental** Fig. 1d**, Supplemental** Fig. 2).[20] Bone marrow monocytes in both groups exhibited reduced levels of macrophage marker F4/80, indicative of a reduced differentiation state.[22] By contrast, CXCR2, TREM2, and CD168 levels were only moderately impacted in *Ticam2*$^{-/-}$ CS-injected mice, suggesting a mild deviation from the typical exhaustion phenotype.

To measure inflammatory cytokine expression in CS-injected mice, we performed qRT-PCR on column-purified bone marrow monocytes. Interestingly, despite evidence of tolerized *Tnf* and *Il12a* expression in WT CS-injected mice, *Tnf*, *Il1b*, and *Il12a* expression were all elevated in *Ticam2*$^{-/-}$ CS-injected mice (Fig. 1c). Thus, *Ticam2* deletion prevented the development of tolerance, potentially allowing monocytes to mount a more effective response to septic challenge that may in part account for the increased survival of *Ticam2*$^{-/-}$ mice.

Monocyte exhaustion in sepsis patient samples

To test the fidelity of our mouse CS model of monocyte exhaustion, we performed time course flow cytometry analyses on human blood samples collected between 1 to 4 days after sepsis onset using a novel 20-factor exhaustion phenotyping panel. After gating for the monocyte lineage (CD15^{-};SSC^{low};CD11b^{+};CD14/16^{+}),

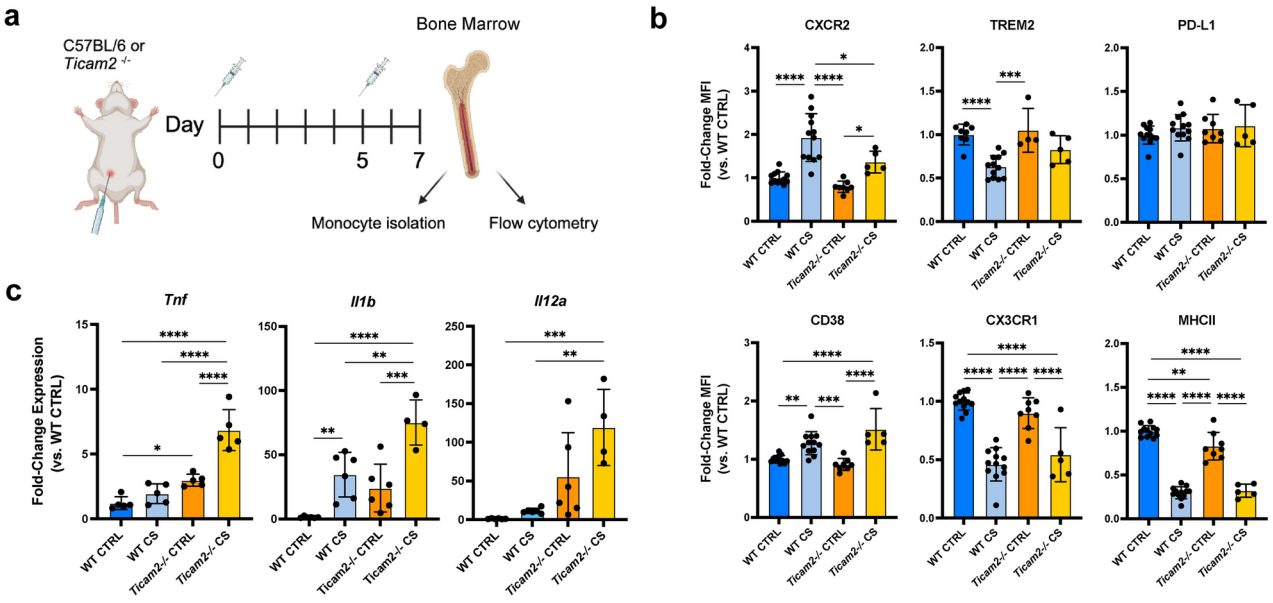

Fig. 1. *Ticam2* deletion enables sustained inflammatory activity in septic monocytes. (**a**) Experimental paradigm for mouse cecal slurry (CS) injection experiments. Following intraperitoneal CS injections on day 0 and 5, bone marrow cells isolated from septic mice were analyzed by flow cytometry or subjected to LS column purification of bone marrow monocytes. (**b**) Flow cytometry mean fluorescence intensity (MFI) values for monocyte exhaustion markers in bone marrow monocytes relative to WT control (CTRL). Dots represent individual mice, with mean MFI and SD indicated (n = 4–12; one-way ANOVA with Tukey's multiple comparisons test; ****p-adj < 0.0001; ***p-adj < 0.001; **p-adj < 0.01; *p-adj < 0.05). (**c**) qRT-PCR for inflammatory cytokine expression in bone marrow monocytes relative to WT CTRL (n = 4–6; one-way ANOVA with Holm-Šídák's multiple comparisons test; mean and SD indicated).

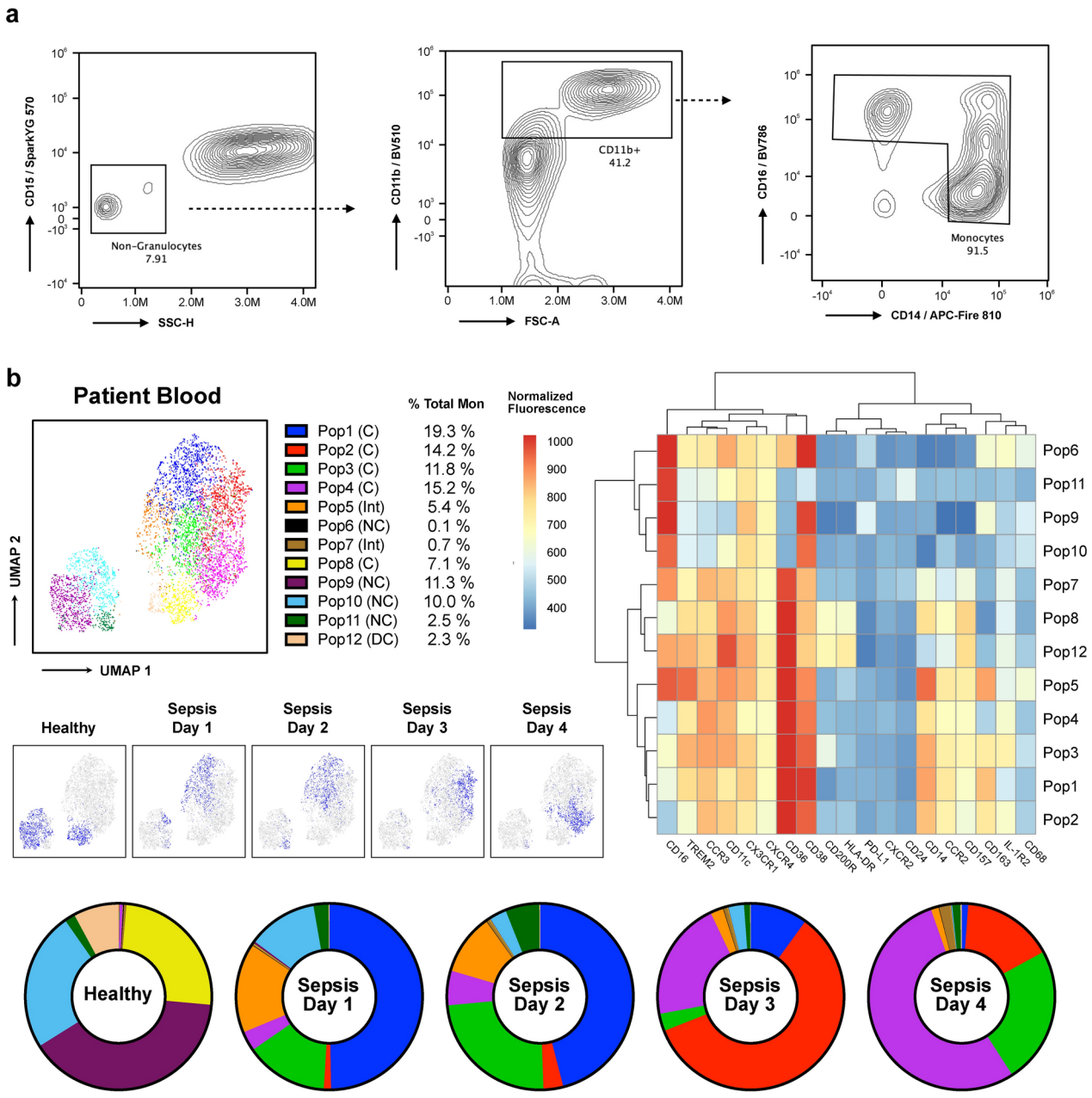

Fig. 2. Expansion of exhausted blood monocytes in sepsis patients. (**a**) Flow cytometry gating strategy for human blood monocytes (**b**) FlowSOM analysis of human blood monocyte populations in time course sepsis patient samples or healthy volunteers. Circle diagrams indicate the average proportions of each FlowSOM population in a given condition, while correlation heatmaps depict the normalized fluorescence intensity for each marker within a population. Populations are broadly categorized as classical (C), non-classical (NC), or intermediate (Int) monocytes or dendritic cells (DC).

cells from the sepsis patient or healthy volunteers were analyzed using flow self-organizing map (FlowSOM) automated cell clustering to identify populations enriched at each time point (Fig. 2a-b, **Supplemental Table 1**).[23] Cells clustered into 12 distinct populations (Pop) split between four categories: 1) Classical (C; Pop1, 2, 3, 4, and 8), 2) Non-classical (NC; Pop6, 9, 10, and 11), 3) Intermediate (Pop5 and 7), and 4) Dendritic cells (Pop12). A rapid and progressive depletion of NC populations was observed in sepsis patient samples in favor of C populations, which comprised 95% of monocyte lineage cells by Day 4. In addition, we noted an early, transient expansion of intermediate monocytes (Pop5), as was previously reported for sepsis patients.[24,25] A gradual shift in the phenotype of C monocytes was also apparent over the course of sepsis progression. Early sepsis time points enriched for the closely related Pop1 and Pop3, which exhibit elevated levels of scavenger receptor CD163 and either suppressed Il-1R2 expression (Pop1) or increased CD200R (Pop3). At Day 3, C monocytes were primarily comprised of Pop2 cells, a transitional population with reduced TREM2 expression.

By Day 4, however, roughly half of all monocyte lineage cells belong to Pop4, which gradually expanded over the course of sepsis progression. Unlike healthy donor C monocytes (Pop8), Pop4 cells are depleted of MHCII isotype HLA-DR and CX3CR1 and express elevated levels of CD38, all salient features of exhausted monocytes and consistent with our mouse CS model.[11,12,21].

Ticam2$^{-/-}$ monocytes exhibit perturbed sepsis epigenetic memory

Loss of TICAM2 signaling impairs the acquisition of LPS-driven monocyte epigenetic memory in the form of 5mC.[20] To measure the impact of *Ticam2* deletion on 5mC reprogramming in monocytes during sepsis, we analyzed genomic DNA methylation levels in column-purified bone marrow monocytes 48 h after sepsis onset using Infinium Mouse Methylation BeadChip arrays.

Similar to WT CS monocytes, significant hypomethylation was observed at CpGs across the genome in *Ticam2* CS-injected mice (**Supplemental** Fig. 3a).[20] Differentially methylated region (DMR) modeling identified 21,344 hypomethylated and 2,973 hypermethylated CpG sites in *Ticam2*$^{-/-}$ CS vs. *Ticam2*$^{-/-}$ control (CTRL) bone marrow monocytes (Fig. 3a-b**, Supplemental Table 2**). Roughly 50% of these DMR sites were shared with WT CS monocytes, although *Ticam2*$^{-/-}$ monocytes exhibited a greater number of hypermethylated regions. Probe annotation and chromatin state discovery and characterization (chromHMM) analyses identified enhancers and transcription start site flanking regions as heavily enriched among DMRs in *Ticam2*$^{-/-}$ CS monocytes, supporting the regulatory potential of altered DNA methylation in these cells (**Supplemental** Fig. 3b**, Supplemental Table**

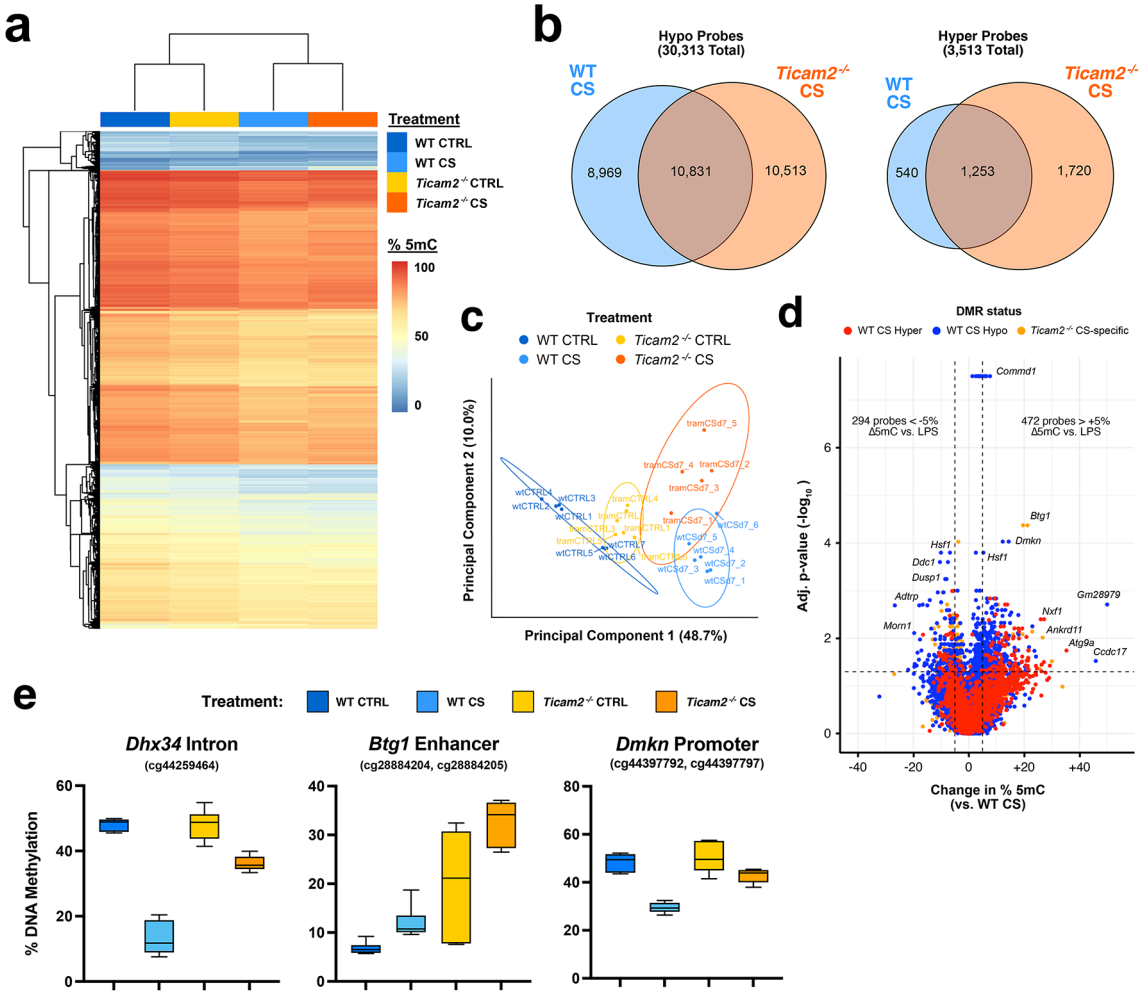

Fig. 3. Altered DNA methylation reprogramming in septic *Ticam2*$^{-/-}$ monocytes. (**a**) Correlation heatmap for average DNA methylation at differentially methylated CpG probes in bone marrow monocytes collected from CTRL or CS day 7 mice (≥ 5% difference in percent 5mC versus WT or *Ticam2*$^{-/-}$ CTRL; FDR < 5%; n = 5–7 mice for each group). (b) Venn overlap of DMR probes in WT and *Ticam2*$^{-/-}$ CS monocytes. (c) PCA of DMR probes. Ovals indicate normal distribution for each group. (d) Volcano plot for altered DNA methylation at DMR probes in *Ticam2*$^{-/-}$ CS monocytes versus WT CS. Probes are colored based on observed DMR patterns observed in WT CS monocytes (red = hypermethylated, blue = hypomethylated) or differential methylation observed in *Ticam2*$^{-/-}$ CS monocytes alone (orange). Dotted lines indicate the change in methylation (≥ 5%) and adjusted p value (< 0.05) cutoffs for DMRs. (e) Representative DMRs with altered methylation in *Ticam2*$^{-/-}$ CS monocytes versus WT CS.

3). Consistent with this observation, several transcription factors known to play important immunomodulatory roles in monocytes were significantly enriched at differentially methylated CpGs in *Ticam2*$^{-/-}$ CS monocytes, including JUNB, CEBPE, MLLT3, and IRF8 (**Supplemental** Fig. 3c).[26–29] Gene ontology (GO) enrichment analysis of nearest linked genes also identified an enrichment for numerous immune pathways, including IL-3, IL-5, IL-6, and IL-2 signaling among hypomethylated DMRs (**Supplemental Table 4**).

Hierarchical clustering and principal components analyses indicated that while *Ticam2*$^{-/-}$ CS monocytes most closely resembled WT CS cells, their DNA methylome profile was distinct from all other groups tested (Fig. 3a,c). To more thoroughly evaluate methylome differences between these two groups, we re-performed DMR modeling of *Ticam2*$^{-/-}$ CS monocytes versus WT CS. Focusing on probes that exhibit significant methylation differences relative to their respective control groups, we identified 766 CpG probes with significantly altered DNA methylation in *Ticam2*$^{-/-}$ CS monocytes relative to WT CS (Fig. 3d**, Supplemental Table 2**). Of those regions, 354 demonstrated evidence of rescue such that DNA methylation levels in *Ticam2*$^{-/-}$ CS monocytes more closely resembled CTRL cells. Among these regions was restored methylation at an intronic enhancer for *Dhx34*, an RNA helicase involved in nonsense-mediated decay regulation, and in the promoter of *Dmkn*, a secreted factor most well-known for its role in epidermal inflammatory signaling (Fig. 3e).[30,31] We also noted increased methylation at an enhancer linked to the anti-proliferative factor *Btg1* unique to *Ticam2*$^{-/-}$ monocytes.[32] Finally, transcription factor motif enrichment revealed a significant increase in CEBPE binding sites among hypomethylated CpG probes in *Ticam2*$^{-/-}$ CS monocytes relative to WT, while hypermethylated probes exhibited significant enrichment for members of the JUN/FOS and IRF families (**Supplemental Table 3**).

Taken together, these data suggest that loss of TICAM2 signaling results in a unique DNA methylation signature in septic monocytes, with potential implications for the long-term behavior of these cells resulting from altered innate immune memory.

Loss of Ticam2 facilitates monocyte exhaustion recovery following sepsis resolution

Septic challenge can result in the functional impairment of monocytes beyond their typical lifespan of 1 to 7 days, suggesting long-term changes to central immune memory in the form of monocyte exhaustion.[14,33–35] To test the recovery of monocyte behavior following sepsis resolution, we performed flow cytometry on WT and *Ticam2*$^{-/-}$ bone monocytes one week after CS injection when cells are expected to have undergone one full turnover. Strikingly, while the proportion of monocytes among bone marrow cells was elevated in both groups, the incidence of "intermediate" subtype monocytes remained high in WT mice but normalized to control levels in *Ticam2*$^{-/-}$ animals (**Supplemental** Fig. 4a-b).

To rigorously phenotype bone marrow monocyte subpopulations, we performed FlowSOM automated cell clustering on monocytic lineage cells (Fig. 4a**, Supplemental Table 1**). In agreement with our standard gating strategy, WT CS bone cells are dominated by a Population 5 (Pop5), a lowly-differentiated Ly6C-intermediate depleted of CX3CR1; this was reflected in reduced mean cell surface CX3CR1 levels on all WT CS monocytes (**Supplemental** Fig. 4c). A similar late-expanding CX3CR1-deficient monocyte population was identified in a mouse cecal ligation puncture sepsis model, and was shown to increase mortality risk following secondary infection.[13] By contrast, CTRL and *Ticam2*$^{-/-}$ CS bone marrow samples exhibited a greater proportion of Pop2 cells, a Ly6C-high subset with high cell surface CX3CR1 levels. Lastly, whereas WT CS bone marrow was completely depleted of anti-inflammatory Ly6C-low Pop14 cells, there was a trend toward increased Pop14 levels in *Ticam2*$^{-/-}$ CS samples.

Next, we sought to characterize splenic reservoir monocytes following one week of CS recovery. Like bone marrow, spleen monocyte levels were elevated in WT and *Ticam2*$^{-/-}$ mice relative to control (**Supplemental** Fig. 4a). However, in contrast to bone marrow, *Ticam2*$^{-/-}$ CS mice most closely resembled WT CS based on their expanded proportion of Ly6C-high monocytes and reduced levels of Ly6C-intermediate and -low subpopulations (**Supplemental** Fig. 4b). FlowSOM analysis revealed a high degree of similarity between WT and *Ticam2*$^{-/-}$ CS spleen monocytes, with elevated levels of Ly6C-high Pop4 cells and diminished contributions from Ly6C-low Pop1 and Pop5 (Fig. 4b**, Supplemental Table 1**). Of particular interest, was the increased incidence of Pop10 cells unique to the CS condition. These monocytes exhibit the paradoxical pro-inflammatory, anti-immune (CD38^{high}; PD-L1^{high}) profile characteristic of exhausted monocytes in addition to reduced CX3CR1 cell surface levels.[12] Whereas Pop10 cells accounted for 25% of WT CS splenic monocytes, the incidence was reduced to 13% in *Ticam2*$^{-/-}$ CS mice, suggesting a trend toward an improvement in the immune profile of *Ticam2*$^{-/-}$ mice following sepsis. This effect was also observable in the reduced average CD38 and PD-L1 signals of *Ticam2*$^{-/-}$ CS monocytes relative to WT CS (**Supplemental** Fig. 4d). Taken together with results from bone marrow, these data support an accelerated recovery from monocyte exhaustion in *Ticam2*$^{-/-}$ mice following sepsis resolution.

Finally, to test persistence of the exhausted monocyte phenotype during monocyte differentiation, we harvested bone marrow monocytes from WT and *Ticam2*$^{-/-}$ mice one week after CS injection and cultured them for five days in the presence of M-CSF. After four days of culture, cells were treated with PBS control or high-dose LPS (100 ng/mL) media for 24 h and analyzed by flow cytometry for key exhaustion markers. Under PBS control conditions, most monocytes transitioned to a Ly6C-low or -intermediate cell state, although there was a reduction of Ly6C-intermediate cells in WT CS cultures (Fig. 5a). By contrast, LPS stimulation resulted in an expansion in pro-inflammatory Ly6C-high monocytes with elevated PD-L1, CD38, and CD86 in WT monocytes (Fig. 5b). Notably, CD86 activation was suppressed while CD38 levels were significantly increased in WT CS monocytes, supporting the persistence of the exhaustion phenotype during lineage differentiation. By contrast, although *Ticam2*$^{-/-}$ monocytes are hyporesponsive to LPS stimulation, a concomitant increase in CD38 activation was not observed in CS cells relative to CTRL. We also performed qRT-PCR to measure the expression of key cytokines following LPS stimulation. Whereas *Tnf* expression was unimpacted in CS monocytes, evidence of immune tolerance was observable in the reduced expression of *Il1b*, *Il6*, and *Il12a* in WT CS cells (Fig. 5c). A similar effect was not observed in *Ticam2*$^{-/-}$ CS cultures, but this may have been masked by the low responsivity

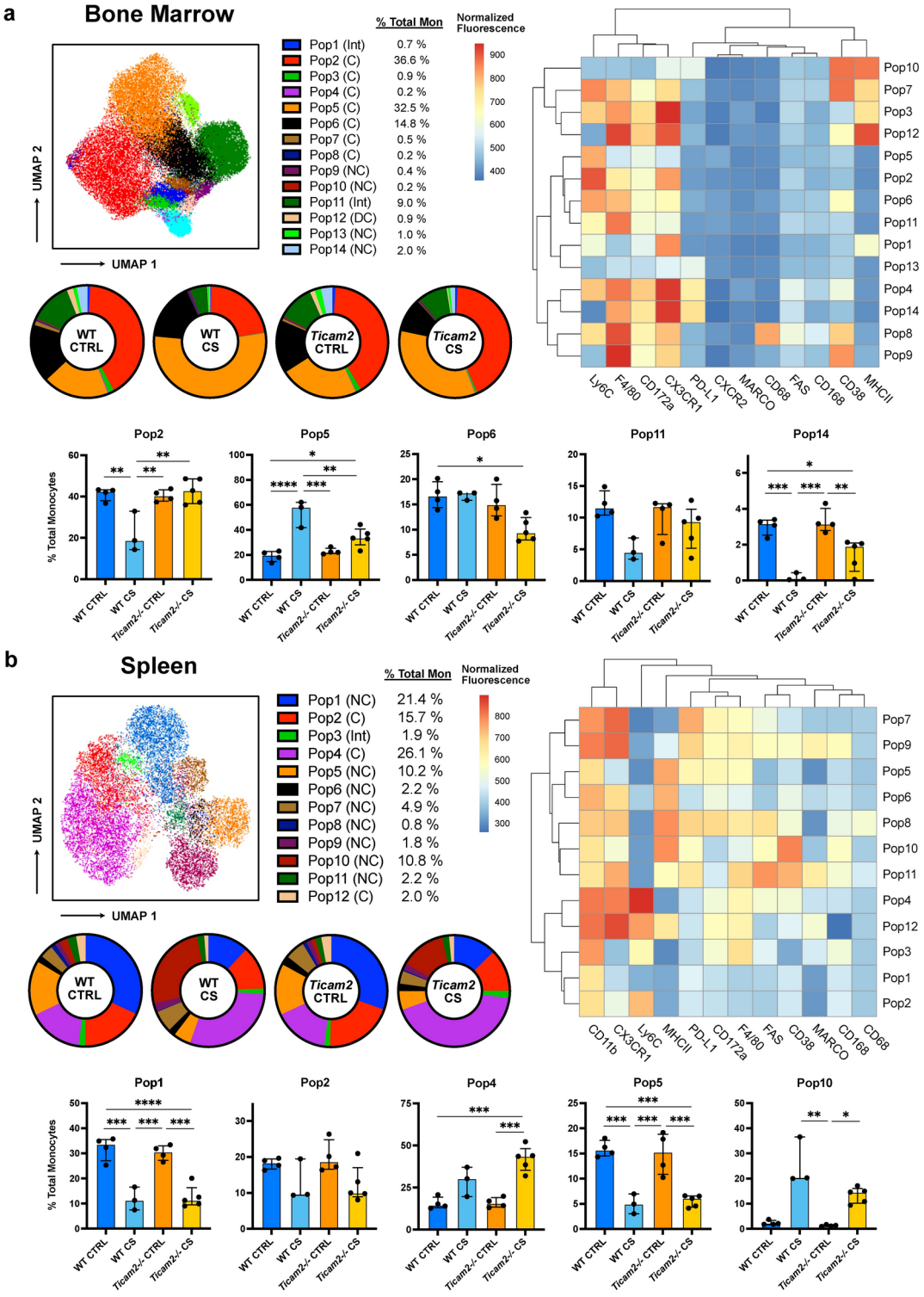

Fig. 4. *Ticam2* deletion facilitates monocyte exhaustion resolution during sepsis recovery. (**a**-**b**) FlowSOM analysis of bone marrow (**a**) and splenic (**b**) monocyte populations in CS recovery mice. Circle diagrams indicate the average proportions of each FlowSOM population in a given condition, while correlation heatmaps depict the normalized fluorescence intensity for each marker within a population. Populations are broadly categorized as classical (C), non-classical (NC), or intermediate (Int) monocytes or dendritic cells (DC). Bar graphs depict the incidence of major FlowSOM population across biological replicates, with median percentages and IQR indicated (n = 3–5; one-way ANOVA with Tukey's multiple comparisons test for BM Pop2, 5, and 14 and Spleen Pop1, 4, and 5; non-parametric Kruskal–Wallis with Dunn's multiple comparisons test for BM Pop6 and 11 and spleen Pop2 and 10; ****p-adj < 0.0001; ***p-adj < 0.001; **p-adj < 0.01; *p-adj < 0.05).

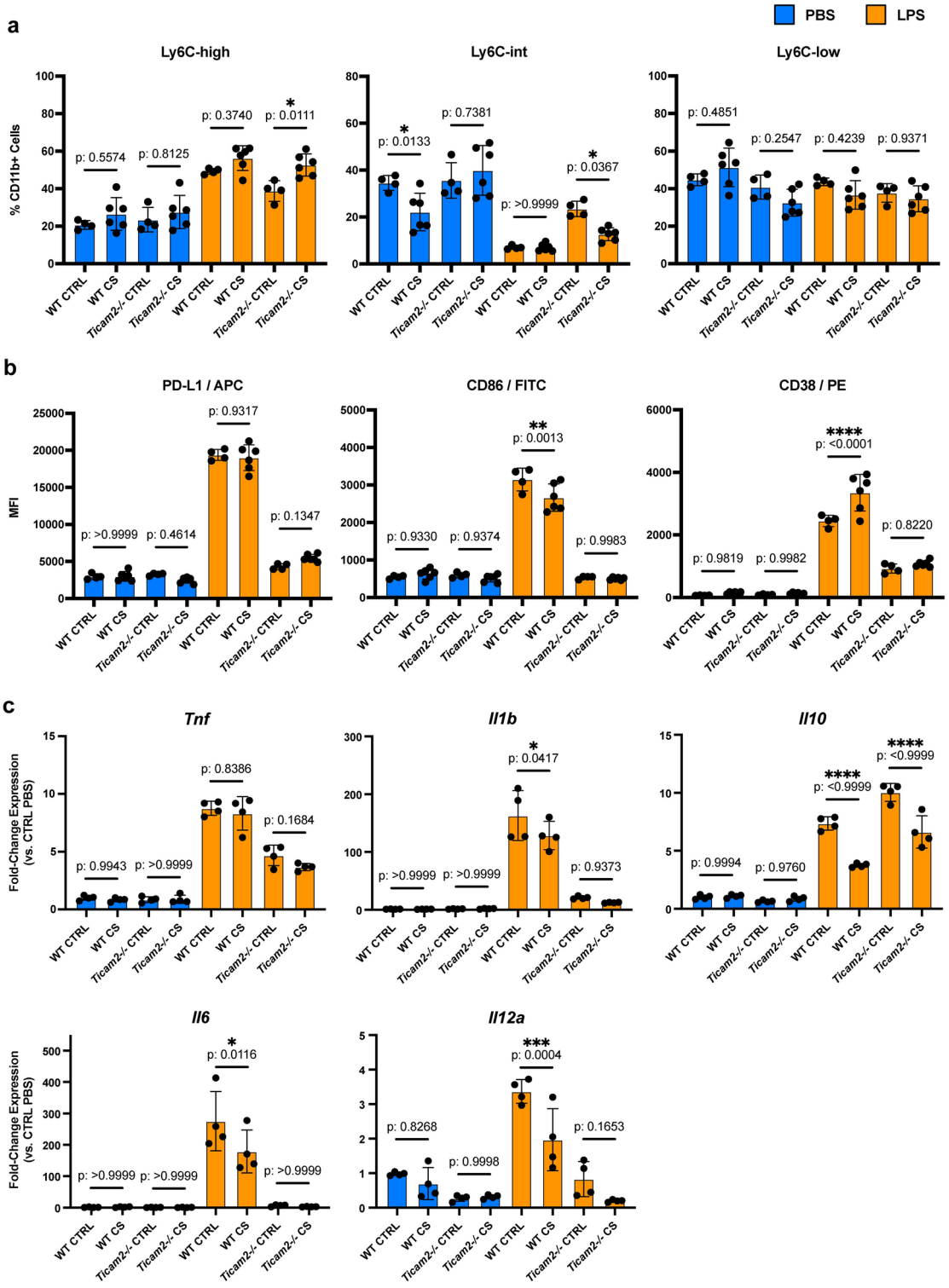

Fig. 5. Monocyte exhaustion persists in cultured BMMCs derived from CS recovery mice. (**a**) Percentages of Ly6C subtypes in BMMCs cultured from CS recovery mice. Dots represent individual cultures derived from separate mice, with mean percentages and SD indicated (n = 4; one-way ANOVA with Šidák's multiple comparisons test; ****p-adj < 0.0001; ***p-adj < 0.001; **p-adj < 0.01; *p-adj < 0.05). (**b**) Flow cytometry mean fluorescence intensity (MFI) values for monocyte exhaustion markers in cultured BMMCs (n = 4; one-way ANOVA with Šidák's multiple comparisons test). (**c**) qRT-PCR for cytokine expression in cultured BMMCs relative to WT CTRL (n = 4–6; one-way ANOVA with Šidák's multiple comparisons test).

of *Ticam2*$^{-/-}$ cells to LPS stimulation. However, both WT and *Ticam2*$^{-/-}$ CS monocytes exhibited reduced *Il10* activation following LPS treatment, suggesting these cells preserve some of the features associated with sepsis-induced tolerance.[36].

Discussion

Monocyte exhaustion is a hallmark feature of sepsis pathogenesis that limits the immune system's capacity to mount effective responses to future infections.[4,12,37] Time course blood samples from a septic patient revealed a rapid, early expansion of classical and intermediate monocytes that eventually transitioned into a CX3CR1^{low}; HLA-DR^{low}; CD38^{high} exhausted state. A similar effect was observed in the bone marrow of CS-challenged mice, suggesting exhaustion is not restricted to peripheral tissues and may impact central immune memory. Consistent with this model, bone marrow samples collected after one week of sepsis recovery revealed that most monocytes in WT CS mice persist in a Ly6C-intermediate, CX3CR1^{low} state. By contrast, *Ticam2*$^{-/-}$ CS bone marrow evidenced an increase in classical Ly6C-high, CX3CR1^{high} monocytes to control levels, supporting an accelerated recovery of central immune memory in these mice.

Long-term changes to innate cell behavior following immune challenge, termed innate immune memory, are driven in large part by alterations to the epigenome of affected cells.[38–40] Previous work from our group demonstrated that DNA methylation represents an underexplored facet of monocyte exhaustion, with thousands of sites across the genome undergoing in dynamic 5mC reprogramming in response to septic challenge.[20] Whereas a similar phenomenon of genome-wide hypomethylation was observed in bone marrow monocytes of *Ticam2*$^{-/-}$ CS mice, these cells also exhibited an expansion of hypermethylated regions and altered DNA methylation at regulatory sites for key immune genes such as *Btg1* and *Dmkn*. While neither factor has been studied in the context of sepsis progression, both have been shown to participate in the cell-autonomous modulation of myeloid development and inflammatory activity.[41–44] We also noted a rescue of DNA methylation levels in the promoter of *Dhx34*, an RNA helicase involved in nonsense-mediated decay and pre-mRNA splicing during myeloid differentiation.[45] Finally, we observed an enrichment for CEBPE binding sites among DMRs hypomethylated in *Ticam2*$^{-/-}$ CS bone marrow monocytes relative to WT CS. CEBPE plays several critical roles in myeloid behavior during infection, including regulation of *Il6*, *Il10*, and *Il12a* expression, all of which were notably impacted in exhausted monocytes.[46,47] Given that CEBPE itself is characterized as a methyl-insensitive transcription factor, increased recruitment of CEBPE to DMRs in *Ticam2*$^{-/-}$ monocytes may function to pioneer open chromatin regions or maintain them in an unmethylated state.[48,49].

Previous studies have focused on immunostimulation and innate immune training as a means of treating long-term immunosuppression in sepsis survivors.[5,6,50–52] It therefore seems paradoxical that accelerated recovery of monocyte exhaustion was achieved through TICAM2 ablation, which represents a major inflammatory circuit in the TLR4 signaling apparatus.[53–55] Notably, *Ticam2* deletion preferentially impacted the tolerogenic effect of sepsis on monocyte cytokine expression during the early phase of sepsis pathogenesis. In contrast, loss of TICAM2 seems to impact persistent maintenance of the exhausted memory state. Similarly, neutrophils harvested from *Ticam2*$^{-/-}$ mice following one week of sepsis recovery were previously shown to exhibit heightened expression of pro-resolving markers and reduced endothelial disruption compared to WT mice, arguing for a pan-myeloid role for TICAM2 in regulating long-term innate immune memory.[56] This is likely achieved through one of three potential mechanisms. First, loss of TICAM2 signaling may inhibit the establishment of long-term central immune memory in the form of chromatin alterations, as was observed with altered DNA methylation in *Ticam2*$^{-/-}$ CS monocytes. Second, loss of TICAM2 signaling may render CS monocytes hyporesponsive to immune challenges, titrating their response to immune challenge during both phases of sepsis pathogenesis in a manner that favors rapid recovery. Finally, given the whole-body knockout of *Ticam2*, we cannot discount that loss of TICAM2 in stromal or adaptive immune cells affects paracrine signaling cues that would otherwise maintain monocytes in an exhausted state.[57–60].

Several experimental limitations are notable in our study. First, we cannot exclude that loss of *Ticam2* signaling impacts hematopoiesis or baseline inflammatory signaling to alter monocyte exhaustion in sepsis-challenged mice. While the high degree of similarity observed in the cell surface profiles of WT and *Ticam2*$^{-/-}$ control monocytes (Fig. 4a-b) argues against these interpretations, conditional knockout and pharmacological models will be needed to address whether accelerated exhaustion recovery upon TICAM2 inhibition is translatable to human patients.[12] We also noted higher expression of inflammatory cytokines *Tnf*, *Il1b*, and *Il12a* in *Ticam2*$^{-/-}$ monocytes, likely due to diminished tolerogenesis in these mice. Such elevated inflammatory activity may contribute to more rapid bacterial clearance, but it also increases the risk for organ damage during the systemic inflammation phase of sepsis pathogenesis. Although cecal slurry-challenged *Ticam2*$^{-/-}$ mice were previously shown to be protected from lung and endothelial barrier damage due to increased pro-resolving neutrophil activity, this remains an important consideration for any future TICAM2-based interventions.[56] Finally, we would like the note that our human sepsis patient data is limited to a single case study and may not reflect broader differences among septic patients. Since the initiation of our study, clinical sepsis definitions have changed reflecting the poor overlap between SIRS and sepsis, yet these features were used as inclusion criteria in our report. We also acknowledge a lack of functional testing for tolerance inception in patient blood samples, although diminished HLA-DR levels relative to healthy controls suggests tolerogenesis preceded our Day 1 blood collection. Further testing will be necessary to more accurately capture innate immune memory onset in septic patients.

In summary, long-term monocyte exhaustion is a conserved feature of sepsis-derived immunosuppression in mice and human patients. Genetic ablation of TICAM2 signaling altered the establishment of innate immune epigenetic memory and effected a more rapid recovery of exhausted monocytes in CS-challenged mice relative to wild-type controls. TICAM2 inhibition therefore presents significant therapeutic potential for the treatment of long-term immunosuppression in sepsis survivors.

Methods

Mice

Wild-type (C57BL/6) mice were purchased from The Jackson Laboratory. *Ticam2*$^{-/-}$ mice were provided by Dr. Holger Eltzschig (University of Texas Houston) and regularly maintained in our laboratory. Sex- and age-matched animals of 6 to 8 weeks were used for this study. Mice were housed in a pathogen-free facility with 12–12 h light–dark cycles and free access to water and standard chow. All mouse experiments were approved by the Institutional Animal Care and Use Committee of Virginia Tech (protocol 21–038) in accordance with ARRIVE guidelines 2.0 and the U.S. National Institutes of Health Guide for the Care and Use of Laboratory Animals.

Clinical samples and inclusion criteria

As a case study, we collected serial blood draws from 70-year-old female pneumonia patient presenting with septic shock upon ICU entry (**Supplemental Table 6**). The study inclusion criteria are adult patients 18 years of age or older suspected to be septic by either: 1) Fulfilling systemic inflammatory response syndrome (SIRS) criteria, which includes heart rate > 90 bpm, respiratory rate > 20 breaths/min, WBC > 12,000 or < 4,000, bands > 10%, and temperature > 100.9°F or < 96.8°F, or 2) Having a positive quick Sequential Organ Failure Assessment (qSOFA). A qSOFA score is considered positive if 2 or more of the following criteria are met: respiratory rate ≥ 2 breaths/min, systolic blood pressure ≤ 100 mmHg, or Glasgow Coma Score ≤ 13. Exclusion criteria for this study include patients with a presenting hemoglobin of < 9.0 mg/dL, evidence of active bleeding, concern for hemorrhagic shock or having received blood transfusion within the past 90 days, patients with an active or past medical history of white blood cell disorders, patients whose first set of blood cultures were drawn over 24 h prior to enrollment, pregnant patients, and patients who are currently imprisoned or incarcerated. Patient blood cultures were drawn within 24 h of inclusion, and blood samples from anonymous healthy donors were used as a control. Blood samples were processed through erythrocyte sedimentation in 3% dextran and followed by ACK lysis (Quality Biological). Residual leukocytes were washed in fetal bovine serum (FBS; TCB) and applied to flow cytometry. All experiments were approved by a joint Institutional Review Board through Virginia Tech and Carillion Roanoke Memorial Hospital (protocol 20–823). Samples were collected with the written informed consent of all participants or their legal guardian. It was conducted and performed in compliance with the ethical standards set out in the Declaration of Helsinki.

Cecal slurry preparation and injections

Sepsis was induced by intraperitoneal CS injections as previously described.[61] Whole ceca were dissected from 12-week-old C57BL/6 mice, and cecal contents were extracted, mixed with sterile water (250 µg/µL), sequentially filtered through 860 µm and 190 µm mesh strainers, mixed with equal volume 30% glycerol in PBS, and placed in -80˚C storage. For CS injections, frozen CS stock was rapidly thawed and injected into the peritoneal cavity of recipient mice (0.9 mg/g mouse weight). After 5 days, mice were injected with a second 0.9 mg/g CS dose, and then euthanized by cervical dislocation 2 or 7 days later. Bone marrow cells were collected as previously described.[12] Splenocytes were obtained through mechanical disruption of whole spleen followed by enzymatic digestion (100 U/mL Collagenase IV, 20 U/mL DNAseI, 1% FBS in HBSS) and 70 µm filtration. Bone marrow monocytes were isolated through LS column purification (Miltenyi #130–042-401) according to the manufacturer's protocol.

Cell culture

Bone marrow cells harvested from mice after one week of CS recovery were seeded on CELLSTAR 6-well plates (Greiner #657,160) at a density of 3×10^5 cells/cm^2 and cultured in complete RPMI 1640 media (10% FBS, 1% penicillin–streptomycin, 1% L-glutamine) supplemented with 10 ng/mL macrophage colony-stimulating factor (M-CSF; PeproTech #315–02). Cells were cultured for 5 days at 37˚C in a humidified 5% CO_2 atmosphere with fresh media changes at day 2 and 4 of culture. On day 4, cell were treated with high-dose 100 ng/mL lipopolysaccharide (LPS; Sigma-Aldrich #L2630) or PBS for 24 h, after which cells were collected using a cell scraper.

Flow cytometry

Primary mouse bone marrow cells and splenocytes or day 5 cultured BMMCs were washed in PBS and blocked in 1:100 Fc block (BD Biosciences #553,142) for 20 min at 4˚C. Cells were then incubated for 30 min at 4˚C in one of two panels. Primary cells were stained with antibodies against Ly6C (RRID:AB_1732079, clone HK1.4), CD11b (RRID:AB_2738184, clone M1/70), Ly6G (Elabscience #E-AB-F1108I, clone 1A8), CXCR2 (R&D Systems #FAB2164G, clone 242,216), CD68 (RRID:AB_2910295, clone FA-11), CD172a (RRID:AB_2739912, clone P84), CX3CR1 (RRID:AB_2565700, clone SA011F11) F4/80 (RRID:AB_2734769, clone T45-2342), CD38 (RRID:AB_2871855, clone 90/CD38), PD-L1 (RRID:AB_2738911, clone MIH5), MARCO (R&D Systems # FAB29561R, clone 2359A), FAS (RRID:AB_2728202, clone SA367H8), MHCII (RRID:AB_2191073, clone M5/114.15.2), CD168 (RRID:AB_2927540), and TREM2 (R&D Systems # FAB17291N, clone 237,920). Cultured BMMCs were stained with antibodies against Ly6C (RRID:AB_1732093, clone HK1.4), CD11b (RRID:AB_830641, clone M1/70), CD86 (RRID:AB_313162, clone PO3), PD-L1 (RRID:AB_3083280, clone MIH6), and CD38 (RRID:AB_312928, clone 102,707). All antibodies were incubated at 1:100 dilutions with the exceptions of CD172a (1:50) and PD-L1 (1:200). Cells were then washed with FACS buffer (HBSS with 2% fetal bovine serum, FBS) and resuspended in FACS buffer containing propidium iodide (Invitrogen #00–6990-42). For human PBMCs, cells were blocked in TruStain FcX (Biolegend #422,301) for 20 min at 4˚C and then incubated for 30 min with 1:100 dilutions of antibodies against CD11b (RRID:AB_2629529, clone M1/70), CD11c (RRID:AB_1595430, clone Bu15), CD16 (RRID:AB_2744299, clone 3G8), CD14 (RRID:AB_2860953, clone 63D3), CD68 (Bioss # bs-1432R-A680), CD200R (RRID:AB_2564351, clone OX-108), CD15 (AB_2927951,

clone W6D3), CX3CR1 (RRID:AB_2743987, clone 2A9-1), HLA-DR (RRID:AB_893574, clone L243), Il-1R2 (RRID:AB_2609075, clone 34,141), CD163 (RRID:AB_2573722, clone GHI/61), CD24 (RRID:AB_314853, clone ML5), CD36 (RRID:AB_2072511, clone 5–271), CD38 (RRID:AB_2894562, clone S17015F), PD-L1 (RRID:AB_2802211, clone MIH1), CD157 (RRID:AB_3068112, clone W21007F), CXCR2 (Novus # NBP1-43338AF532, clone 5E8-C7-F10), CXCR4 (Novus # NBP1-77067MFV610), CCR2 (RRID:AB_2800969, clone K036C2), and TREM2 (Novus # NBP1-07101PECY7, clone 2B5). Mouse and human primary cells were measured with an Aurora 4L 16 V-14B-10YG-8R (Cytek), while cultured BMMCs were measured with a FACS Canto II (BD Biosciences).

Quantitative real-time PCR (qRT-PCR)

Total RNA was extracted using a RNease Plus Mini Kit (QIAGEN #74,134) and reverse transcribed using a High-Capacity cDNA Reverse Transcription Kit (Applied Biosystems #4,368,813) according to the manufacturer's protocol. qRT-PCR was performed using Power SYBR Green Master Mix (Thermo Fisher #4,368,702) on a CFX96 Real-Time System C1000 Thermal Cycler (Bio-Rad). Relative expression levels were determined using the Pffafl method normalized to the mean of genes *Actb* and *Oaz1*. Melt curve analyses were performed for each sample to exclude false positives. Primer information is available in Supplemental Table 7.

Infinium Mouse Methylation BeadChip array

Genomic DNA was prepared from cultured monocytes using a DNeasy Blood & Tissue Kit (QIAGEN #69,504), bisulfite-treated using an EpiTect Bisulfite Kit (QIAGEN #59,104), and processed and hybridized to individual array wells of an Infinium Mouse Methylation BeadChip (Illumina), as previously described.[20] All samples were processed and run at the Children's Hospital of Philadelphia Center for Applied Genomics.

Flow cytometry analysis

All flow cytometry data were analyzed in FlowJo (BD Life Sciences). No further fluorescence compensation was performed beyond the standard Cytek spectral deconvolution workflow. For FlowSOM analyses, individual biological replicates for each condition were downsampled to ensure equal contribution of all conditions (with a minimum downsample size of 1000 live cells), and then cells were clustered using FlowSOM (Set Seed = 3). Cell clusters were visualized using the FlowJo UMAP plugin to assess clustering fidelity and spatial distribution. For BMMC culture experiments, a minimum of 5000 live cells were analyzed for each condition.

Infinium BeadChip array analysis

Raw Infinium IDAT files were processed into corrected beta values using the openSesame pipeline (1.14.2; default parameters), and differentially methylated regions (DMRs) were identified using the sesame DML function.[62] Wild-type CS day 7 bone marrow monocyte array values were previously published, but were collected and sequenced at the same time as *Ticam2*$^{-/-}$ samples (GEO: GSE242816).[20] Infinium BeadChip probe annotations, including transcription factor motif enrichment and chromatin state discovery and characterization (chromHMM), were obtained using the sesame KYCG function.[62] For gene ontology enrichment, differentially methylated probes were matched to their nearest gene and ontology enrichment was performed using the g:Profiler2 package (0.2.1).[63] Average DNA methylation signal and unsupervised clustering heatmaps were prepared using the Rpackage pheatmap (1.0.12; https://www.rdocumentation.org/packages/pheatmap; clustering_method = "average"), and average signal violin plots were prepared using the Rpackage vioplot (0.4.0; https://github.com/TomKellyGenetics/vioplot). Principal components analysis was performed using the R stats package.

Statistics

General statistics were performed using Prism 10 (Graphpad). Normal distributions were examined using the Shapiro–Wilk test. For normally distributed data, comparisons between > 3 groups were performed using one-way ANOVA adjusted for Tukey's multiple comparisons, while paired comparisons between control and CS groups were corrected using Šídák's method based on the assumption that each comparison is independent of the other. For data not normally distributed, comparisons between > 3 groups were performed using Kruskal–Wallis adjusted for Dunn's multiple comparisons. Statistical significance is accepted for adjusted p-values < 0.05.

Data availability

Raw and processed DNA methylation array data produced during this study are available through the Gene Expression Omnibus under the accession number GSE271939.

Received: 10 September 2024; Accepted: 8 January 2025
Published online: 15 January 2025

References

1. Liang, L., Moore, B. & Soni, A. National Inpatient Hospital Costs: The Most Expensive Conditions by Payer, 2017. *Healthcare Cost and Utilization Project (HCUP) Statistical Briefs* (2020).
2. Rudd, K. E. et al. Global, regional, and national sepsis incidence and mortality, 1990–2017: analysis for the Global Burden of Disease Study. *The Lancet* **395**, 200–211 (2020).
3. Gaieski, D. F., Edwards, J. M., Kallan, M. J. & Carr, B. G. Benchmarking the incidence and mortality of severe sepsis in the United States. *Crit. Care. Med.* **41**, 1167–1174 (2013).
4. Hotchkiss, R. S., Monneret, G. & Payen, D. Sepsis-induced immunosuppression: from cellular dysfunctions to immunotherapy. *Nat. Rev. Immunol.* **13**, 862–874 (2013).

5. Torres, L. K., Pickkers, P. & Van Der Poll, T. Sepsis-Induced Immunosuppression. *Annu. Rev. Physiol.* **84**, 157–181 (2022).
6. Venet, F. & Monneret, G. Advances in the understanding and treatment of sepsis-induced immunosuppression. *Nat. Rev. Nephrol.* **14**, 121–137 (2017).
7. Haveman, J. W. et al. The central role of monocytes in the pathogenesis of sepsis: consequences for immunomonitoring and treatment. *Neth. J Med.* **55**, 132–141 (1999).
8. Cavaillon, J. M. & Adib-Conquy, M. Monocytes/macrophages and sepsis. *Crit. Care Med.* **33**, S506–S509 (2005).
9. Chousterman, B. G., Swirski, F. K. & Weber, G. F. Cytokine storm and sepsis disease pathogenesis. *Semin. Immunopathol.* **39**, 517–528 (2017).
10. Rigato, O. & Salomao, R. Impaired production of interferon-gamma and tumor necrosis factor-alpha but not of interleukin 10 in whole blood of patients with sepsis. *Shock* **19**, 113–116 (2003).
11. Venet, F. et al. Decreased monocyte human leukocyte antigen-DR expression after severe burn injury: Correlation with severity and secondary septic shock. *Crit. Care Med.* **35**, 1910–1917 (2007).
12. Pradhan, K., Yi, Z., Geng, S. & Li, L. Development of exhausted memory monocytes and underlying mechanisms. *Front. Immunol.* **12**, 778830 (2021).
13. Baudesson de Chanville, C. et al. Sepsis triggers a late expansion of functionally impaired tissue vascular inflammatory monocytes during clinical recovery. *Front. Immunol.* https://doi.org/10.3389/fimmu.2020.00675 (2020).
14. Shalova, I. N. et al. Human monocytes undergo functional re-programming during sepsis mediated by hypoxia-inducible factor-1α. *Immunity* **42**, 484–498 (2015).
15. Monneret, G. et al. Persisting low monocyte human leukocyte antigen-DR expression predicts mortality in septic shock. *Intensive Care Med.* **32**, 1175–1183 (2006).
16. Lekkou, A., Karakantza, M., Mouzaki, A., Kalfarentzos, F. & Gogos, C. A. Cytokine production and monocyte HLA-DR expression as predictors of outcome for patients with community-acquired severe infections. *Clin. Diagn. Lab. Immunol* **11**, 161–167 (2004).
17. Landelle, C. et al. Low monocyte human leukocyte antigen-DR is independently associated with nosocomial infections after septic shock. *Intensive Care Med.* **36**, 1859–1866 (2010).
18. Wang, J., Wu, Y., Lin, R. C., Zhang, Y. & Li, L. TRAM deletion attenuates monocyte exhaustion and alleviates sepsis severity. *Front. Immunol.* **14**, 1297329 (2023).
19. Naler, L. B. et al. Epigenomic and transcriptomic analyses reveal differences between low-grade inflammation and severe exhaustion in LPS-challenged murine monocytes. *Commun. Biol.* **5**, 1–17 (2022).
20. Caldwell, B. A., Wu, Y., Wang, J. & Li, L. Altered DNA methylation underlies monocyte dysregulation and immune exhaustion memory in sepsis. *Cell Rep.* **43**, 113894 (2024).
21. Pachot, A. et al. Decreased expression of the fractalkine receptor CX3CR1 on circulating monocytes as new feature of sepsis-induced immunosuppression. *J. Immunol.* **180**, 6421–6429 (2008).
22. Austyn, J. M. & Gordon, S. F4/80, a monoclonal antibody directed specifically against the mouse macrophage. *Eur. J. Immunol.* **11**, 805–815 (1981).
23. Van Gassen, S. et al. FlowSOM: Using self-organizing maps for visualization and interpretation of cytometry data. *Cytom. Part A* **87**, 636–645 (2015).
24. Hortová-Kohoutková, M. et al. Differences in monocyte subsets are associated with short-term survival in patients with septic shock. *J. Cell Mol. Med.* **24**, 12504–12512 (2020).
25. Mukherjee, R. et al. Non-Classical monocytes display inflammatory features: validation in sepsis and systemic lupus erythematous. *Sci. Rep.* **5**, 1–14 (2015).
26. Calvanese, V. et al. MLLT3 governs human haematopoietic stem-cell self-renewal and engraftment. *Nature* **576**, 281–286 (2019).
27. Reyes, M. et al. An immune-cell signature of bacterial sepsis. *Nat. Med.* **26**, 333–340 (2020).
28. Kurotaki, D. et al. Essential role of the IRF8-KLF4 transcription factor cascade in murine monocyte differentiation. *Blood* **121**, 1839–1849 (2013).
29. Fontana, M. F. et al. JUNB Is a key transcriptional modulator of macrophage activation. *J. Immunol.* **194**, 177–186 (2015).
30. Utsunomiya, A. et al. Homeostatic Function of Dermokine in the Skin Barrier and Inflammation. *J. Investig. Dermatol.* **140**, 838-849.e9 (2020).
31. Hug, N. & Cáceres, J. F. The RNA helicase DHX34 activates NMD by promoting a transition from the surveillance to the decay-inducing complex. *Cell Rep.* **8**, 1845–1856 (2014).
32. Kim, S. H., Jung, I. R. & Hwang, S. S. Emerging role of antiproliferative protein BTG1 and BTG2. *BMB Rep.* **55**, 380 (2022).
33. Yona, S. et al. Fate mapping reveals origins and dynamics of monocytes and tissue macrophages under homeostasis. *Immunity* **38**, 79–91 (2013).
34. van Furth, R. & Cohn, Z. A. The origin and kinetics of mononuclear phagocytes. *J. Exp. Med.* **128**, 415–435 (1968).
35. Patel, A. A. et al. The fate and lifespan of human monocyte subsets in steady state and systemic inflammation. *J. Exp. Med.* **214**, 1913–1923 (2017).
36. Randow, F. et al. Mechanism of endotoxin desensitization: involvement of interleukin 10 and transforming growth factor beta. *J. Exp. Med.* **181**, 1887–1892 (1995).
37. Caldwell, B. & Li, L. Epigenetic regulation of innate immune dynamics during inflammation. *J. Leukoc. Biol.* **115**, 589–606 (2024).
38. Quintin, J., Cheng, S. C., van der Meer, J. W. M. & Netea, M. G. Innate immune memory: towards a better understanding of host defense mechanisms. *Curr. Opin. Immunol.* **29**, 1–7 (2014).
39. Smale, S. T., Tarakhovsky, A. & Natoli, G. Chromatin Contributions to the Regulation of Innate Immunity. *Annu. Rev. Immunol.* **32**, 489–511 (2014).
40. Netea, M. G. et al. Defining trained immunity and its role in health and disease. *Nat. Rev. Immunol.* **20**, 375–388 (2020).
41. Suk, K., Sipes, D. G. & Erickson, K. L. Enhancement of B-cell translocation gene-1 expression by prostaglandin E2 in macrophages and the relationship to proliferation. *Immunology* **91**, 121–129 (1997).
42. Il, J. C., Ae, K. L., Song, J. L., Myung, G. L. & Kim, S. G. Repression by oxidative stress of iNOS and cytokine gene induction in macrophages results from AP-1 and NF-κB inhibition mediated by B cell translocation gene-1 activation. *Free Radic. Biol. Med.* **39**, 1523–1536 (2005).
43. Frentzel, S. et al. IκBNS-deficiency protects mice from fatal Listeria monocytogenes infection by blunting pro-inflammatory signature in Ly6Chigh monocytes and preventing exaggerated innate immune responses. *Front. Immunol.* **13**, 1028789 (2022).
44. Zhang, Z., Bossila, E. A., Li, L., Hu, S. & Zhao, Y. Central gene transcriptional regulatory networks shaping monocyte development in bone marrow. *Front. Immunol.* **13**, 1011279 (2022).
45. Hug, N. et al. A dual role for the RNA helicase DHX34 in NMD and pre-mRNA splicing and its function in hematopoietic differentiation. *RNA* **28**, 1224–1238 (2022).
46. Tavor, S. et al. Macrophage functional maturation and cytokine production are impaired in C/EBPε-deficient mice. *Blood* **99**, 1794–1801 (2002).
47. Cheng, S. et al. The function and regulation of CCAAT/enhancer binding protein ε. *Eur. J. Inflamm.* https://doi.org/10.1177/1721727X231153322 (2023).
48. Héberlé, É. & Bardet, A. F. Sensitivity of transcription factors to DNA methylation. *Essays Biochem.* **63**, 727–741 (2019).
49. Yin, Y. et al. Impact of cytosine methylation on DNA binding specificities of human transcription factors. *Science* https://doi.org/10.1126/science.aaj2239 (2017).

50. Novakovic, B. et al. β-Glucan reverses the epigenetic state of LPS-induced immunological tolerance. *Cell* **167**, 1354-1368.e14 (2016).
51. Gill, P. S., Ozment, T. R., Lewis, N. H., Sherwood, E. R. & Williams, D. L. Trained immunity enhances human monocyte function in aging and sepsis. *Front. Immunol.* **13**, 872652 (2022).
52. Liu, D. et al. Sepsis-induced immunosuppression: mechanisms, diagnosis and current treatment options. *Mil. Med. Res.* **9**, 1–19 (2022).
53. Verstak, B. et al. The TLR signaling adaptor TRAM interacts with TRAF6 to mediate activation of the inflammatory response by TLR4. *J. Leukoc. Biol.* **96**, 427–436 (2014).
54. Oshiumi, H. et al. TIR-containing Adapter Molecule (TICAM)-2, a Bridging Adapter Recruiting to Toll-like Receptor 4 TICAM-1 That Induces Interferon-β. *J. Biol. Chem.* **278**, 49751–49762 (2003).
55. Yamamoto, M. et al. TRAM is specifically involved in the Toll-like receptor 4–mediated MyD88-independent signaling pathway. *Nat. Immunol.* **4**, 1144–1150 (2003).
56. Lin, R. C. et al. Resolving neutrophils due to TRAM deletion renders protection against experimental sepsis. *Inflamm. Res.* **72**, 1733–1744 (2023).
57. Yao, Y. et al. Induction of autonomous memory alveolar macrophages requires t cell help and is critical to trained immunity. *Cell* **175**, 1634-1650.e17 (2018).
58. Hamada, A., Torre, C., Drancourt, M. & Ghigo, E. Trained immunity carried by non-immune cells. *Front. Microbiol.* **10**, 423772 (2019).
59. Niec, R. E., Rudensky, A. Y. & Fuchs, E. Inflammatory adaptation in barrier tissues. *Cell* **184**, 3361–3375 (2021).
60. Crowley, T., Buckley, C. D. & Clark, A. R. Stroma: the forgotten cells of innate immune memory. *Clin. Exp. Immunol.* **193**, 24–36 (2018).
61. Starr, M. E. et al. A New cecal slurry preparation protocol with improved long-term reproducibility for animal models of sepsis. *PLoS One* **9**, e115705 (2014).
62. Zhou, W., Triche, T. J., Laird, P. W. & Shen, H. SeSAMe: Reducing artifactual detection of DNA methylation by Infinium BeadChips in genomic deletions. *Nucleic Acids Res.* **46**, 123 (2018).
63. Peterson, H., Kolberg, L., Raudvere, U., Kuzmin, I. & Vilo, J. Gprofiler 2 -- an R package for gene list functional enrichment analysis and namespace conversion toolset g: profiler. *F1000 Res* https://doi.org/10.12688/f1000research.24956.1 (2020).

Acknowledgements

The authors would like to thank Yajun Wu, Jing Wang, and Yao Zhang for assistance with mouse cecal slurry injections and dissections and Feng Xu for mouse colony management. We would also like to thank technicians at the Children's Hospital of Philadelphia center for Applied Genomics for their service in DNA methylation array analyses. This work was supported by the National Institutes of Health: 5TL1DK132771 (B.A.C.) and R01-AI-172133 (L.L.). Figure schematics were created using Biorender.com.

Author contributions

Conceptualization, B.A.C. and L.L.; data curation, B.A.C.; formal analysis, B.A.C.; investigation, B.A.C.; visualization, B.A.C.; funding acquisition, B.A.C. and L.L.; writing – original draft, B.A.C.; writing – review & editing, B.A.C., S.I. and L.L.; resources, L.L.; project administration, S.I., A.L., and L.L.; supervision, S.I. and L.L.

Funding

National Institutes of Health,5TL1DK132771,R01-AI-172133

Declarations

Competing interests

The authors declare no competing interests.

Additional information

Supplementary Information The online version contains supplementary material available at https://doi.org/10.1038/s41598-025-86103-x.

Correspondence and requests for materials should be addressed to L.L.